ISSN 2616-5767 Vol.9, Issue 4: 1-12, DOI: 10.25236/AJETS.2026.090401

Correlation Analysis between Load Characteristics of Wind Turbine Blade Root Bolts and Pitch Motor Current

Yaowei Song, Shuyi Yang, Lipeng Peng, Tieqi Zhou

School of Mechanical and Electrical Engineering, Hunan University of Science and Technology, Xiangtan, 411201, China

Abstract: *With the growing trend toward large-scale wind turbines, the loads acting on blade root bolts are becoming increasingly severe. Real-time awareness of their service condition is crucial for ensuring reliable operation of wind turbines. In this paper, a theoretical analysis is first conducted on the load transfer of the wind turbine pitch system and the load characteristics of blade root bolts, and a correlation equation between the pitch motor current and the bolt load is established. Subsequently, a time-domain characteristic analysis of the pitch motor starting current is carried out based on field-measured SCADA data from a wind farm, and the differences in the pitch motor current characteristics before and after blade root bolt fracture are compared. Finally, an electromechanical coupled simulation model incorporating vector control of the pitch motor and load transfer is built using MATLAB /Simulink, and the time-domain characteristic values of the pitch motor starting current under conditions with and without blade root bolt fracture are analyzed. The results show that the fracture of blade root bolts in wind turbines leads to load redistribution and changes in connection stiffness, which consequently results in larger time-domain characteristic values of the pitch motor starting current compared to those under the intact condition.*

Keywords: *Wind turbine, Blade root bolt, Pitch motor current, Load characteristics*

1. Introduction

The rotor of a wind turbine converts wind energy into rotational mechanical energy. In order to precisely regulate wind energy capture and ensure the safety of the turbine, the pitch system adjusts the blade pitch angle to modify the aerodynamic loads, which are then transmitted via the blade root bolts to the hub and the main shaft. As the unit capacity and blade size of wind turbines continue to increase, the alternating and impact loads borne by the blade root bolts become more severe, making their service reliability a key factor determining the overall safety of the turbine.

To date, extensive research on blade root bolts has been conducted by scholars worldwide. On one hand, based on the analysis of load characteristics of blade root bolts, Ouyang Yuxiang et al. [1]analyzed the stress conditions of the blade root bolted connection under extreme operating conditions. Han Wen et al. [2] carried out a dynamic load strength analysis of wind turbine blade root bolts using a turbulence model. Qiu Weidong et al. [3] established a position error model for multi-bolt holes at the blade root and investigated the variation in contact surface stress caused by position errors of different bolt holes at the blade root. Zhipeng et al. [4]derived a theoretical model for calculating the axial force of blade root bolts and validated it through experiments. Long et al. [5]developed a competitive failure model for bolts and proposed a numerical method for determining the critical load of bolt competitive failure under combined excitations. Gao Xinshang et al.[6]further investigated the critical loosening load characteristics of bolts under transverse vibration, providing a reference threshold for the failure warning of bolted connections. Abasolo et al. [7-8] proposed a four-parameter meta-model for estimating the elastic interaction of wind turbine bolts during the tightening process, offering a theoretical basis for accurate bolt assembly.

On the other hand, theoretical support for the service condition monitoring of blade root bolts has been provided. Wang Feng et al. [9] used CIVA software to analyze the effects of refraction angle, wafer size, frequency, and bandwidth on the bolt sound field and defect echoes. Wu Minjie [10]established a blade root bolt condition monitoring model based on operating condition division using clustering and classification algorithms, enabling historical condition partitioning and real-time condition recognition. Han Wen [11] proposed a design scheme for an online monitoring device for wind turbine blade root bolts

ISSN 2616-5767 Vol.9, Issue 4: 1-12, DOI: 10.25236/AJETS.2026.090401

based on the Hall effect and the working principle of unipolar Hall sensors. Zhao Yong et al. [12]conducted regular ultrasonic testing of wind turbine blade bolts and carried out online bolt stress monitoring. Currently, existing sensor-based and ultrasonic methods are still insufficient to support online, non-invasive, and low-cost bolt condition monitoring. In contrast, SCADA data offer a theoretical possibility for low-cost, non-invasive online monitoring, but there is an urgent need to establish the mechanical mapping relationship between SCADA data and blade root bolt loads.

Therefore, in this paper, the blade root bolt group of a wind turbine is taken as the research object, and a systematic study is conducted on the mechanical characteristics of blade root bolts under pitch startup conditions. The intrinsic correlation between blade root bolt loads and pitch motor current is clarified through theoretical analysis. The differences in current characteristics between intact and fractured bolt conditions are mined using wind farm SCADA data. An electromechanical coupled simulation model is established in MATLAB/Simulink, and the mechanical simulation of blade root bolts and the stability analysis of the pitch system under pitch startup conditions are carried out.

2. Theoretical Analysis

2.1 Load Transfer of the Pitch System

When a pitch command is executed by the wind turbine, an output torque is generated by the pitch motor according to the input current I. This torque is transmitted through the three-stage planetary gearbox to the internal gear ring a of the pitch bearing, and then drives the inner ring of the pitch bearing and the blade to rotate, thereby achieving the adjustment of the blade pitch angle. The load transfer of the pitch system is shown in Figure 1.

The driving torque of the pitch motor can be directly calculated from the armature current, and the calculation formula is given as follows [13]:

$$T_a = i_1 i_2 \eta \frac{T_N}{I_N} I \tag{1}$$

Where: T_a is the pitch torque of the motor; i_1 is the reduction ratio of the gearbox; i_2 is the gear transmission ratio; η is the efficiency of the transmission system; T_N and I_N are the rated torque and rated current of the motor, respectively; I is the pitch motor current.

The torque balance relationship during the pitch startup process can be expressed as:

$$T_a - T_b - T_f = 0 \tag{2}$$

Where: T_b is the blade pitching torque; T_f is the friction torque of the pitch bearing.

Therefore, under pitch startup conditions, the friction torque T_f of the pitch bearing is approximately constant, and thus the fluctuation of the motor pitching torque T_a directly reflects the variation of the blade pitching torque T_b.

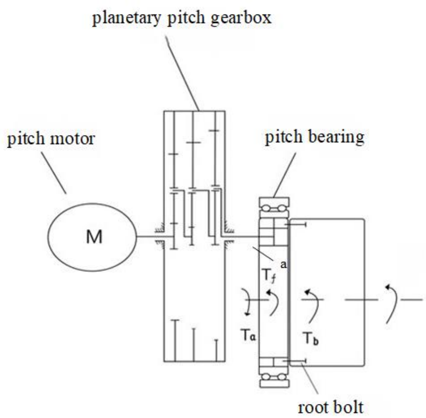

Fig.1 Load transfer of the pitch system

ISSN 2616-5767 Vol.9, Issue 4: 1-12, DOI: 10.25236/AJETS.2026.090401

2.2 Mechanical Analysis of the Blade Root Bolt Connection

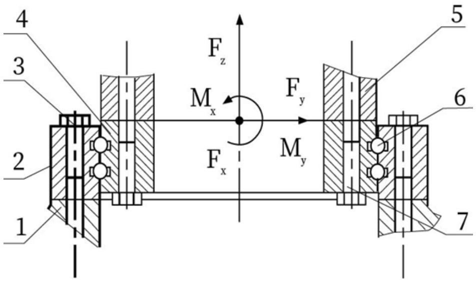

1. Hub; 2. Bearing outer ring; 3. Outer ring bolt; 4. Bearing inner ring; 5. Blade root; 6. Bearing rolling element; 7. Blade root bolt

Fig. 2 Force diagram of the blade root [2]

During the operation of a wind turbine, the blades are subjected to aerodynamic loads, gravitational loads, inertial loads, centrifugal loads, and Coriolis loads [14]. These loads are transmitted through the blade, the blade root bolts, and the pitch bearing to the hub. In the blade root coordinate system, the aforementioned loads can be decomposed into the flapwise moment M_x, the edgewise moment M_y, the torsional moment M_z, the horizontal loads F_x and F_y, and the axial load F_z. Under non-pitching conditions of the wind turbine, the effects of the torsional moment M_z and the horizontal loads F_x and F_y on the forces at the blade root are very small and can be neglected. A simplified force diagram of the blade root is shown in Figure 2 [2].

When the blade root bolts are subjected to an overturning moment M (i.e., the resultant moment of M_x and M_y), the relationship between the bolt axial force F_a and the overturning moment M is expressed as:

$$F_a = \frac{M}{R^2 \sum_{i=1}^{n} (\sin \theta_i)^2} r_i = \frac{4M}{\mathrm{R}n} \tag{3}$$

Where R is the diameter of the pitch circle of the blade root bolts, θ_i is the angular position of the bolt, and n is the number of bolts.

Since the load exerted by the axial load F_z on the blade root bolts is uniformly distributed, the expression is:

$$F_a = \frac{F_z}{n} \tag{4}$$

When the blade root bolts are simultaneously subjected to the overturning moment M and the axial load F_z, the relationship is expressed as:

$$F_a = \frac{4M}{Rn} \pm \frac{F_z}{n} \tag{5}$$

Under pitching conditions of the wind turbine, when the blade root bolts are subjected to a torque M_z, the relationship between the shear force F_q on the blade root bolts and the torque M_z is expressed as:

$$F_q = \frac{M_z}{Rn} \tag{6}$$

By combining Equations (1), (2), and (6), the pitch motor current can be linked to the stress state of the blade root bolts:

$$\begin{cases} T_a = i_1 i_2 \eta \dfrac{T_N}{I_N} I \\ T_a - T_b - T_f = 0 \\ F_q = \dfrac{M_z}{Rn} \end{cases} \tag{7}$$

Based on the above analysis, under non-pitching conditions of the wind turbine, the effects of the torque M_z and the horizontal loads F_x and F_y at the blade root on the forces of the blade root are weak and can be neglected. Under pitching conditions, however, the effect of the torque induced by blade pitching on the blade root bolts cannot be ignored. According to the combined relationship expressed in Equation (7), a clear correspondence exists between the motor pitching torque $\mathrm{T_a}$ and the motor current I;

ISSN 2616-5767 Vol.9, Issue 4: 1-12, DOI: 10.25236/AJETS.2026.090401

therefore, the variation of the motor pitching torque T_a can be obtained through the monitoring of the pitch motor current I. When the friction torque T_f of the pitch bearing remains relatively constant, the fluctuation of T_a mainly reflects the variation of the blade pitching torque T_b. The blade pitching load, as an external load, is directly transmitted to the bolted connection structure of the blade root, where the torque M_z is converted into the shear force on the bolts. Thus, it can be seen that during the pitch startup process of the wind turbine, the variation of the pitch motor current I is intrinsically related to the stress state of the blade root bolts. By monitoring the fluctuation of the pitch motor current, the stress variation of the blade root bolts can be indirectly characterized to a certain extent.

3. SCADA Data Analysis

3.1 Current Characteristics under Pitch Startup Conditions

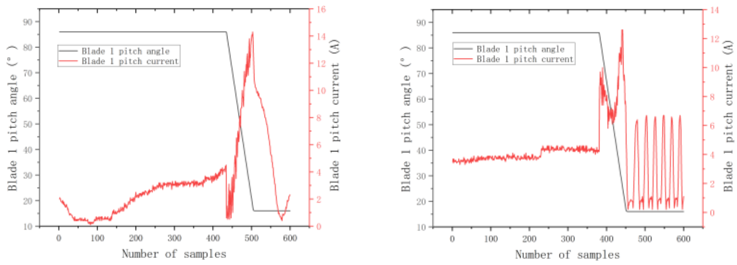

(a) Bolt without fracture *(b) Bolt with fracture*

Fig.3 Raw data of the pitch motor

The SCADA data used in this paper were obtained from the 24-hour continuous operation records of a wind farm over three consecutive days, covering a total of 72 wind turbines with a unit capacity of 2 MW. Among them, blade root bolt fracture occurred in eight units. Data were acquired by the system at a sampling frequency of 1 Hz, and the statistical values were synchronously recorded every 10 minutes. The SCADA data under conditions with and without blade root bolt fracture were extracted, and the 10-minute periods corresponding to the pitch startup stage were screened out. The variation curves of pitch motor current over time for the intact and fractured bolt conditions were plotted, and the results are shown in Figure 3.

Further processing was performed on the data shown in Figure 3, and the time periods during which the pitch angle changed were screened out. The pitch angle values and their corresponding pitch motor current values were extracted from the filtered data. A scatter plot was drawn with the pitch angle on the horizontal axis and the current on the vertical axis, thereby intuitively presenting the correlation between the two. To quantify this relationship, a linear fit was performed on the scatter data, yielding a fitted straight line that reflects the linear trend between the pitch angle and the current, and this line was superimposed on the same coordinate system. As a result, Figure 4 was obtained, which shows the relationship between the pitch angle and the pitch motor current during the pitch startup stage.

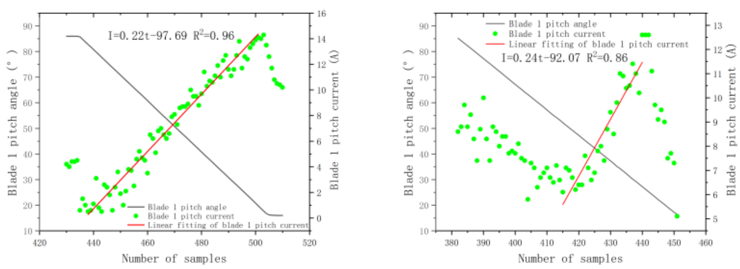

(a) Bolt without fracture *(b) Bolt with fracture*

Fig. 4 Relationship between pitch angle and pitch motor current during the pitch startup stage

As can be seen from the figure, during the pitch startup stage of the wind turbine (where the aerodynamic loads on the blades are negligible), as the pitch angle uniformly changes from 86° to 16°, the pitch current exhibits a linearly increasing or decreasing trend. This phenomenon can be explained as follows: during the pitch startup stage, the rotor is not rotating, and the blades are subjected only to the pitching load caused by gravity. Moreover, due to the different azimuth angles of the blades, the pitching load induced by gravity acts either as an assisting force or as a resisting force.

3.2 Current Characteristics under Intact and Fractured Bolt Conditions

Time-domain and frequency-domain analyses are commonly used methods in engineering signal processing. In equipment condition monitoring, the variation of signals over time is recorded through time-domain analysis. The extracted parameters are classified into dimensional parameters (e.g., maximum value, mean value, root mean square, etc.) and dimensionless parameters (e.g., kurtosis, skewness, etc.). Among them, dimensional parameters are widely adopted due to their computational simplicity, and their common expressions are presented in Table 1.

Tab. 1 Expressions of dimensional characteristic parameters in time domain

Parameter	Expression
Max	$X_1 = max(x_i)$
Min	$X_2 = min(x_i)$
Peak-to-peak value	$X_3 = max(x_i) - min(x_i)$
Mean value	$X_4 = {}^{1}/_{N_s} \sum_{i=1}^{N_s} x_i$
Root mean square(RMS)	$X_5 = \left({}^{1}/_{N_s} \sum_{i=1}^{N_s} (x_i)^2\right)^{0.5}$

Taking the SCADA data of wind turbines under the two operating conditions (intact blade root bolts and fractured blade root bolts) shown in Figure 4 as the research objects, a comparative analysis was conducted. First, a fixed time window method was adopted to segment the continuous signal of the pitch motor current. According to the sampling frequency and the analysis requirements, the window length was set to 10 seconds, and the windows were allowed to overlap or remain non-overlapping as needed to extract local fluctuation characteristics. Within each 10-second window, the peak-to-peak value of the current signal was extracted as the characteristic value, and the results are shown in Figure 5.

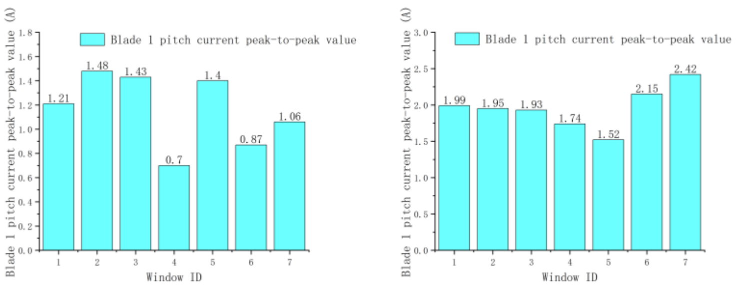

(a) Bolt without fracture *(b) Bolt with fracture*

Fig. 5 Fluctuation amplitude of pitch motor current

As can be seen from Figure 5, under the intact bolt condition, the fluctuation amplitude of the pitch current is relatively small, ranging from 0 to 1.5 A. After the fracture of the blade root bolts, the current fluctuation range is significantly larger than that of the former, with an amplitude exceeding 1.5 A. This indicates that the fracture of the blade root bolts leads to a change in connection stiffness and an intensification of load fluctuations, which in turn causes an increase in the fluctuation amplitude of the pitch current.

4. Mechanical Modeling of Blade Root Bolts and System Stability Analysis

4.1 Pitch Motor Control Model

In this paper, the pitch motor used in the pitch system is a permanent magnet synchronous motor. To facilitate its systematic analysis and modeling, the following simplifying assumptions are usually made [14]: (1) Eddy current and hysteresis losses are neglected; (2) The conductivity of the permanent magnet material is assumed to be zero; (3) No damping windings are arranged on the rotor surface; (4) The back

ISSN 2616-5767 Vol.9, Issue 4: 1-12, DOI: 10.25236/AJETS.2026.090401

electromotive force induced in the stator windings is assumed to have a sinusoidal waveform.

To achieve mathematical model decoupling, the three-phase stationary coordinate system is often transformed into the d-q coordinate system rotating synchronously with the rotor, and the steady-state and dynamic models of the pitch motor are established in this coordinate system. The stator voltage equation can be expressed as:

$$\begin{cases} U_d = R_s i_d + \dot{\varphi}_d + \omega \varphi_q \\ U_q = R_s i_q + \dot{\varphi}_q - \omega \varphi_d \end{cases} \tag{8}$$

Where U_d and U_q are the d- and q-axis stator voltages; i_d and i_q are the d- and q-axis stator currents; R_s is the stator resistance; φ_d and φ_q are the d- and q-axis flux linkages; ω is the electrical angular velocity.

The electromagnetic torque equation is:

$$T_m = \frac{3}{2} p_m \left[\varphi_f i_q + \left(L_d - L_q \right) i_d i_q \right] \tag{9}$$

The mechanical dynamics equation is:

$$J_e \dot{\omega}_m = T_m - T_l - B\omega_m \tag{10}$$

Where P_m is the number of pole pairs of the pitch motor; J_e is the moment of inertia of the pitch motor; ω_m is the mechanical angular velocity of the pitch motor; B is the damping coefficient of the pitch motor; and T_l is the load torque.

The pitch motor (PMSM) vector control system adopts the id=0 control strategy. Its overall structure is shown in Figure 6, which is a typical speed-current double closed-loop architecture. After the given speed ω^* is compared with the measured speed ω_m, the reference value of the q-axis current i_q^* is output by the speed PI regulator, while the reference value of the d-axis current i_d^* is set to zero to achieve decoupling. The errors between i_d^*, i_q^* and the actual feedback currents i_d, i_q are processed by the current PI regulators to generate the voltage reference values U_d and U_q. These are then transformed via the inverse Park transformation to obtain U_α and U_β, which are fed into the SVPWM module to generate PWM signals for driving the inverter and controlling the motor operation. Meanwhile, the three-phase currents are sampled and transformed via the Clark and Park transformations to form the current feedback closed loop.

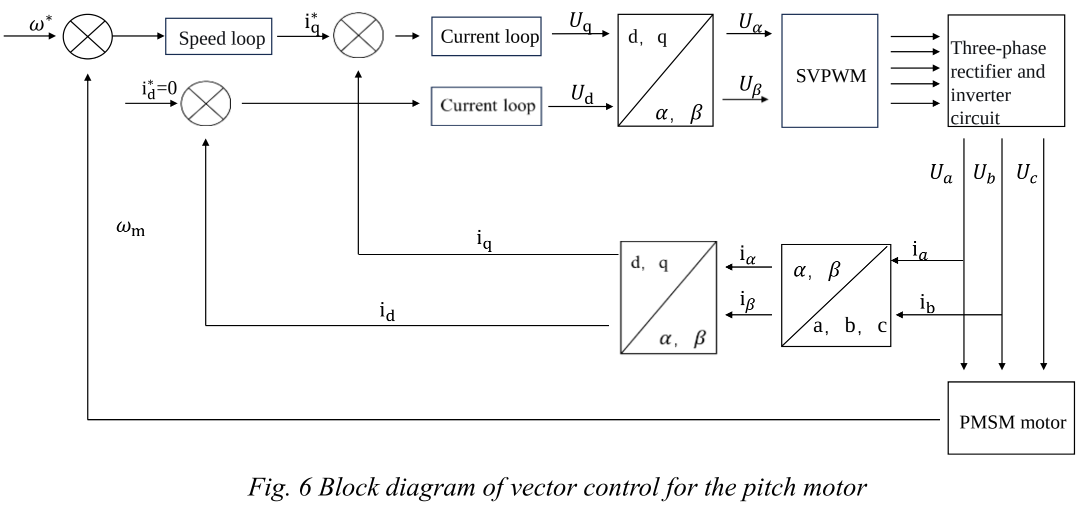

Fig. 6 Block diagram of vector control for the pitch motor

4.2 Mechanical Model of Blade Root Bolts

(1) Under intact condition

The torque T_m output by the pitch motor is transmitted through the drive shaft and the reducer to the pitch bearing, thereby driving the blade to complete the pitching action. The corresponding dynamic model is shown in Figure 7. The motor output shaft is a high-speed shaft, with its torsional stiffness and damping denoted as K_1 and c_1, respectively. The rotational speeds at the two ends of the shaft are $\dot{\theta}_m$ and $\dot{\theta}_1$, and the torsional torque on the high-speed shaft is T_1. The output shaft of the reducer is a low-

ISSN 2616-5767 Vol.9, Issue 4: 1-12, DOI: 10.25236/AJETS.2026.090401

speed shaft, with its stiffness and damping denoted as K_2 and c_2, respectively. The shaft rotational angles are θ_2 and θ_3, and the torsional torque on the low-speed shaft is T_2 . The reduction ratio of the reducer is i_1, and the torque is further converted into the pitch driving torque T_a through the internal gear ring of the pitch bearing, with a transmission ratio of i_2 at this stage. The moments of inertia of the pitch motor, reducer, gear transmission mechanism, and the pitch bearing connection system are J_m, J_1, J_2, and J_3, respectively. The magnitude of the high-speed shaft torque T_1 is determined by the difference in rotational angles at its two ends (θ_m-θ_1); similarly, the magnitude of the low-speed shaft torque T_2 depends on the difference in rotational angles (θ_2-θ_3), while the magnitude of the pitch driving torque is determined by the difference in rotational angles $(\theta_4 - \theta_5)$. The system vibration differential equations are given as follows:

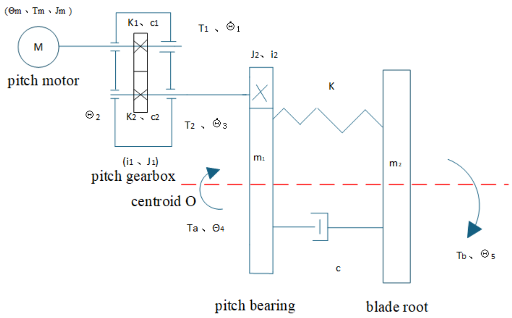

Fig. 7 Dynamic model of the pitch system

$$\begin{cases} T_m - T_1 = J_m\ddot{\theta}_m \\ K_1(\theta_m - \theta_1) + c_1(\dot{\theta}_m - \dot{\theta}_1) = T_1 \\ K_2(\theta_2 - \theta_3) + c_2(\dot{\theta}_2 - \dot{\theta}_3) = T_2 \\ T_1 - \dfrac{T_2}{i_1} = J_1\ddot{\theta}_1 \\ \dfrac{\dot{\theta}_1}{i_1} = \dot{\theta}_2 \\ T_2 - \dfrac{T_a}{i_2} = J_2\ddot{\theta}_3 \\ \dfrac{\dot{\theta}_3}{i_2} = \dot{\theta}_4 \\ [K(\theta_4 - \theta_5) + c(\dot{\theta}_4 - \dot{\theta}_5)] = T_a \\ T_a - T_b = J_3\ddot{\theta}_5 \end{cases} \tag{11}$$

Under pitching operation, the blade root bolts deform under the action of torque, as shown in Fig. 8.

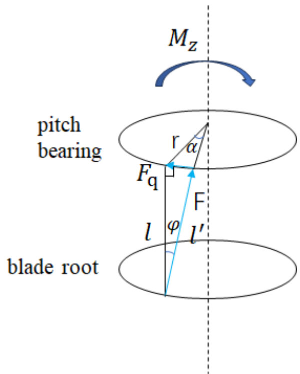

Fig. 8 Torsional deformation model of blade root bolts

Under the applied load, the axial forces F and F′ of the blade root bolt (before and after loading) and the shear force $F_q$form a vector triangle, from which the shear force of the blade root bolt can be obtained as:

$$F_q = F\tan\varphi = k_z l \tan\varphi \tag{12}$$

Where k_z is the connection stiffness of the bolt, l is the original length of the bolt, and φ is the deformation angle.

Assuming that all bolts are uniformly loaded, then

$$M_{Z\mathrm{a}} = F_q \times r \tag{13}$$

Where r is the radius of the pitch circle of the blade root bolts.

According to the geometric relationships in the figure above, it can be known that:

$$l\, tan\, \varphi = \alpha \times r \tag{14}$$

where $\alpha = \theta_4 - \theta_5$ is the relative pitch angle.

By combining all the above equations, the following can be obtained:

$$M_{Z\mathrm{a}} = k_z \alpha r^2 \tag{15}$$

Since during normal pitching of the blade, the bolts are in the elastic deformation stage, the connection stiffness of the bolts remains unchanged and is constant. Moreover, all bolts are uniformly loaded, then:

$$M_Z = nM_{Z\mathrm{a}} = nk_z \alpha r^2 = K\alpha \tag{16}$$

Where K is the equivalent torsional stiffness of the blade root bolt group, and n is the number of blade root bolts.

Combining equations (15) and (16) yields:

$$K = nk_z r^2 \tag{17}$$

Combining equations (11) and (17) yields:

$$\begin{cases} T_m - T_1 = J_e \ddot{\theta}_m \\ K_1(\theta_m - \theta_1) + c_1(\dot{\theta}_m - \dot{\theta}_1) = T_1 \\ K_2(\theta_2 - \theta_3) + c_2(\dot{\theta}_2 - \dot{\theta}_3) = T_2 \\ T_1 - \dfrac{T_2}{i_1} = J_1 \ddot{\theta}_1 \\ \dfrac{\dot{\theta}_1}{i_1} = \dot{\theta}_2 \\ T_2 - \dfrac{T_a}{i_2} = J_2 \ddot{\theta}_3 \\ \dfrac{\dot{\theta}_3}{i_2} = \dot{\theta}_4 \\ \left[K(\theta_4 - \theta_5) + c(\dot{\theta}_4 - \dot{\theta}_5)\right] = T_a \\ T_a - T_b = J_3 \ddot{\theta}_5 \end{cases} \tag{18}$$

$$K = nk_z r^2$$

The blade root bolts can be linked to the pitch transmission equations. The electromagnetic torque output by the pitch motor is affected by the load, and changes in the electromagnetic torque will be reflected in the current.

(2) Under fractured condition of blade root bolts

The pitch bearing is connected to the blade through the blade root bolts. Based on this, a mechanical model for the fracture of the blade root bolts is established, as shown in Figure 9 [15]. After the fracture occurs, the fractured blade root bolts no longer participate in load bearing. Meanwhile, the position of the centroid O of the bolt group is shifted, and the equivalent point of action E of the external load no longer coincides with the centroid O, thereby creating an eccentric distance. After the fracture of the blade root bolts, the failed bolts lose their connection function, and the load is redistributed among the remaining bolts. The remaining bolts remain in a uniformly loaded state, and their deformation is always within the elastic range. The equivalent torsional stiffness of the bolt group decreases linearly, and the shift of the centroid O further induces an additional centrifugal force. Based on this, the mechanical equations for bolt fracture are established as follows:

ISSN 2616-5767 Vol.9, Issue 4: 1-12, DOI: 10.25236/AJETS.2026.090401

$$K = (n - z)k_z r^2 \tag{19}$$

$$T_a - T_b - m\dot{\theta}_5^2 e = J_3 \ddot{\theta}_5 \tag{20}$$

Where z is the number of broken bolts, and e is the eccentric distance.

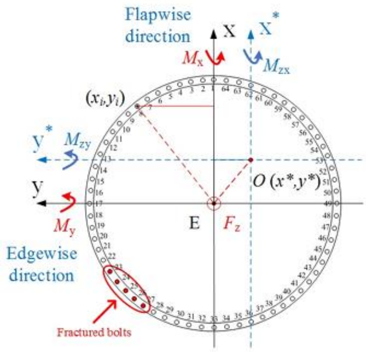

Figure 9 Fracture of blade root bolts[14]

4.3 System Stability Analysis

The pitch system of a 2 MW wind turbine is a torsional damping system, and its dynamic equations can be simplified as:

$$J\ddot{\theta} + B\dot{\theta} + K\theta = \tau_c \tag{21}$$

Where J is the moment of inertia, θ is the torsional angle, B is the damping coefficient, K is the torsional stiffness, and τ_c is the control torque generated by the motor.

Where τ_c is determined by the PI speed controller:

$$\tau_c = K_p(\omega_{ref} - \omega) + K_i \int (\omega_{ref} - \omega)dt \tag{22}$$

In the formula, ω_{ref} is the target rotational speed, and $\omega = \dot{\theta}$ is the actual rotational speed.

The speed error is defined as:

$$e = \omega_{ref} - \omega \tag{23}$$

The integral state is defined as:

$$z = \int edt\, \dot{z} = e \tag{24}$$

Since $\omega = \dot{\theta}$ and $\omega = \omega_{ref} - e$, it follows that:

$$\dot{\omega} = -\dot{e} \tag{25}$$

There are now three state variables: θ, e, and z. The state equations are:

$$\begin{cases} \dot{\theta} = \omega = \omega_{ref} - e \\ \dot{e} = -\dfrac{B + K_p}{J}e - \dfrac{K_i}{J}z + \dfrac{B}{J}\omega_{ref} + \dfrac{K}{J}\theta \\ \dot{z} = e \end{cases} \tag{26}$$

The characteristic equation of the homogeneous system is:

$$det(sI - A) = det\begin{bmatrix} s & 1 & 0 \\ -\dfrac{K}{J} & s + \dfrac{B + K_p}{J} & \dfrac{K_i}{J} \\ 0 & -1 & s \end{bmatrix} = 0 \tag{27}$$

Therefore, there is a pole at zero, $s_1 = 0$;

The remaining two roots are determined by the quadratic equation:

$$s^2+\frac{B+K_p}{J}s+\frac{K_p+K_i}{J}=0 \tag{28}$$

To ensure system stability, all coefficients must be positive.

$$\begin{cases} B+K_p>0 \\ K_p+K_i>0 \end{cases} \tag{29}$$

According to the Routh stability criterion, all coefficients of the characteristic equation of the system are positive (i.e., $B+K_p>0, K_p+K_i>0$), satisfying the necessary condition. However, the existence of a pole at the origin s_1=0 renders the system critically stable, lacking a restoring force for the angular position. Nevertheless, since the controller is designed solely based on the speed error without incorporating position information, this critical characteristic does not affect the achievement of the pitch speed tracking control objective.

5. Simulation Analysis

5.1 Parameter Settings

Based on the mechanical model of the blade root bolts, a complete block diagram of the simulation model system is established, as shown in Figure 10. In this model, the pitch motor part is constructed based on the permanent magnet synchronous motor control model as the theoretical foundation. The gearbox and load part are modeled by combining the dynamic equations of motion. The relevant parameters of the simulation model are set, and the parameters are shown in Table 2.

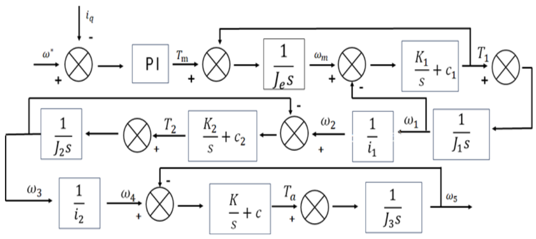

Fig. 10 Block diagram of the simulation model

Tab. 2 Relevant parameters of the simulation model

Parameter	Expression
Inductance parameters L_d(H), L_q(H)	0.003, 0.0035
Motor moment of inertia (kg·m^2)	0.0016
Motor viscous damping (N·m/s)	0
Number of motor pole pairs	4
Reducer reduction ratio	189
Reducer moment of inertia (kg·m^2)	1.5
Motor stator resistance(Ω)	0.25
Reducer high-speed shaft stiffness (N·m)	10000
Reducer high-speed shaft damping (N·m/s)	200
Reducer low-speed shaft stiffness (N·m)	1000000
Reducer low-speed shaft damping (N·m/s)	500
Gear transmission moment of inertia (kg.m^2)	300
Transmission ratio	141/14
Torsional stiffness of blade root bolt group (N·m)	16.64×10^9
Damping of blade root bolt group (N·m/s)	6×10^7
Torsional stiffness of fractured blade root bolt group (N·m)	15.6×10^9
Damping of fractured blade root bolt group (N·m/s)	3×10^7
Eccentric distance(m)	0.066
Blade moment of inertia (kg·m^2)	9.32×10^5

The operating parameters of the simulation model are set as follows: the sampling interval is 1×10^{-6}s, and the simulation duration is set to 40 s, of which the constant-speed motion stage lasts for 35 s. A scope module is added to the simulation model to observe the time-domain signals as they vary over time. Through this module, the variations of signals such as motor speed, pitch angle, and stator current can be monitored in real time.

ISSN 2616-5767 Vol.9, Issue 4: 1-12, DOI: 10.25236/AJETS.2026.090401

5.2 Result Analysis

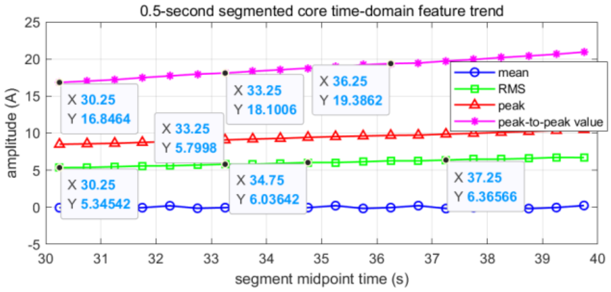

(a)

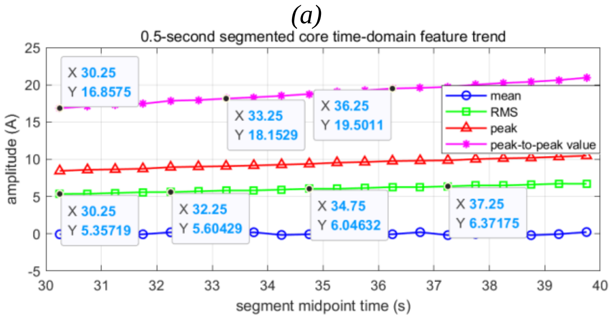

(b)

Fig. 11 Simulated current signals before and after fracture: (a) Simulated current signal with intact bolt (b) Simulated current signal with fractured bolt

A comparative analysis was conducted on the current signals obtained from the simulation model before and after bolt fracture, and their variations were examined from the perspective of time-domain characteristic values. The time-domain characteristics of the current signals before and after bolt fracture are shown in Figure 11. As can be seen from the figure, compared with the intact bolt model, the peak-to-peak current of the fractured bolt model increased by 0.01 A at 30.25 s and by 0.02 A at 36.25 s. This result indicates that the fracture of the blade root bolts induced torque fluctuations in the system, which were reflected in the pitch motor current. However, the magnitude of the current variation is relatively small. The reason is that the established simulation model for bolt fracture did not account for the friction coefficients between the connected and connecting components, thus limiting the calculation accuracy of the model and failing to fully characterize the influence of blade root bolt fracture on the pitch motor current.

6. Conclusion

In this paper, a systematic study is conducted on the load characteristics of the blade root bolt group of a wind turbine under pitch startup conditions. Through theoretical analysis, SCADA data mining, dynamic modeling, and numerical simulation, the following main conclusions are drawn:

(1) The load transfer path of the pitch system is clarified, and the correlation equation between the pitch motor current and the bolt load is established. It is theoretically demonstrated that a mapping relationship exists between the pitch motor current and the bolt load, which provides a theoretical foundation for data-driven condition monitoring.

(2) Based on the field-measured SCADA data from a wind farm, the pitch motor current characteristics during the pitch startup stage are extracted. It is found that the peak-to-peak values of the pitch motor current under the fractured bolt condition are higher than those under the intact bolt condition. When the bolts are intact, the peak-to-peak current is less than 1.5 A; after bolt fracture, the fluctuation increases significantly, and the peak-to-peak values are all greater than 1.5 A.

(3) An electromechanical coupling model incorporating pitch motor control and blade root bolt mechanics is established. The simulation results show that the peak-to-peak current of the fractured bolt model increases by 0.01 A and 0.02 A at 30.25 s and 36.25 s, respectively, compared with the intact bolt model. The underlying mechanism is revealed: bolt fracture leads to a decrease in equivalent torsional stiffness, and the eccentric excitation consequently causes fluctuations in the pitch motor current.

Acknowledgments

The authors gratefully acknowledge the financial supports provided by the Provincial Natural Science Foundation of Hunan, China (No. 2024JJ8274).

References

[1] Ouyang Y.X, Lin N.F, Jin J.T, et al. Static strength design of root connection bolts for large wind turbine blades[J]. Mechanical Engineering and Technology, 2013, 2(3): 87-91.
[2] Han W, Chen C.Z. Dynamic load strength analysis of wind turbine blade root bolts under turbulence model[J]. Journal of Mechanical Strength, 2021, 43(3): 680-685.
[3] Qiu W.D, Wang D.Y, Chen H.X, et al. Study on the influence of position error of blade root bolts on connection stiffness of wind turbine blades[J]. Mechanical Research & Application, 2025, 38(1): 21-25.
[4] Zhipeng L ,Shuyi Y ,Fan Z , et al.Analysis of load characteristics of wind turbine blade root bolts under loosened and fractured conditions[J].Journal of Mechanical Science and Technology, 2024, 38(4):1731-1741.
[5] Yang Long, Yang Bing, Yang Guangwu, et al. Critical-load calculation method of bolt competitive failure under composite excitation[J]. International Journal of Fatigue, 2022, 156.
[6] Gao X.S, Zhou T.M, Mo Y.M, et al. Study on critical loosening displacement load of bolts under transverse vibration[J]. Mechanical Engineering & Automation, 2019(4): 22-27.
[7] Abasolo Mikel, Aguirrebeitia Josu, Avilés Rafael, et al. Methodology for the Optimization of Bolting Sequences for Wind Generator Flanges[J]. Journal of Pressure Vessel Technology, 2014, 136(6).
[8] Abasolo Mikel, Aguirrebeitia Josu, Avilés Rafael, et al. A Tetraparametric Metamodel for the Analysis and Design of Bolting Sequences for Wind Generator Flanges[J]. Journal of Pressure Vessel Technology, 2011, 133(4).
[9] Wang F, Li X.B. Research on in-situ ultrasonic testing of bolts under preload condition[J]. Journal of Railway Science and Engineering, 2021, 18(1): 38-45.
[10] Wu M.J. Research on data-driven condition monitoring of wind turbine blade root bolts[D]. Southwest Jiaotong University, 2023.
[11] Han W. Research on online monitoring of wind turbine blade root bolts based on Hall effect[J]. Mechanical Engineer, 2023(4): 93-95, 99.
[12] Zhao Y, Jiang T, Zhang B.Q, Sun Y, Yang B. Fracture cause analysis of blade bolts of wind turbine generator[J]. Jilin Electric Power, 2020, 48(5): 43-45.
[13] Zhang F, Dai J, Liu D, et al. Investigation of the Pitch Load of Large-Scale Wind Turbines Using Field SCADA Data [J].Energies, 2019, 12(3): 509.
[14] Li T, Yang Q, Peng B. Research on Permanent Magnet Linear Synchronous Motor Control System Simulation[J]. AASRI Procedia, 2012, 3: 262-269.
[15] Li, Zhipeng. Analysis of Load Characteristics of Blade Root Bolt Connection Structure in Wind Turbines. Master's thesis, Hunan University of Science and Technology, 2024.